Deep-Sea Research, Vol. 39, Suppl. 2, pp. S459–S484, 1992.
Printed in Great Britain.

0198–0149/92 $5.00 + 0.00

Internal waves and mixing in the Arctic Ocean

ERIC A. D'ASARO* and JAMES H. MORISON*

(*Received* 25 *January* 1990; *in revised form* 6 *November* 1991; *accepted* 29 *November* 1991)

Abstract—The variability of internal wave shear levels in the eastern Arctic Ocean is explored using velocity profiler and CTD data from Fram Strait and the Nansen Basin. Shear levels are consistently low over the abyssal plains and higher over rougher topography. Applying the parameterization of GREGG (1989, *Journal of Geophysical Research*, **94**, 9686–9698) to these data gives diapycnal diffusivities that vary from about 10^{-6} to above 10^{-4} m s^{-2}. Extrapolating these diffusivities to the entire Arctic Basin suggests that internal wave mixing could play a major role in transporting heat from the warm intermediate water to the surface. Internal wave generation by the barotropic tide on rough topography may explain the higher shear levels found there.

1. INTRODUCTION

THE internal wave climate of the Arctic Ocean, and thus any mixing due to internal waves, differs dramatically from that typically found in other locations. Over most of the world's oceans, the internal wave spectrum is well described by a universal spectrum (GARRETT and MUNK, 1979; LEVINE *et al.*, 1985), here referred to as "GM." In the Arctic Ocean, however, the internal wave field appears to be far more variable. Early measurements by YEARSLEY (1966), NESHYBA *et al.* (1972), and LEVINE *et al.* (1985) indicated that the internal wave energy under the pack ice is one to two orders of magnitude lower than that typically found in the open ocean. Measurements made during the Arctic Internal Wave Experiment (AIWEX) in the Canada Basin of the Arctic Ocean show energy levels 10–20 times less than GM and squared shear levels about seven times less (D'ASARO and MOREHEAD, 1991; LEVINE *et al.*, 1987). In the Fram Strait region, however, much larger values have been found. SANDVEN and JOHANNESSEN (1987) analysed thermistor chain data from MIZEX 83 and found internal wave kinetic energies lower than the GM spectrum by a factor of only 2–3. FOSTER and ECKERT (1987) similarly found levels only slightly less than GM.

One of the most important questions regarding internal waves in the Arctic is what effect they have on the transfer of heat in the basin. The heat budget of the Arctic Ocean (AAGAARD and GREISMAN, 1975) is dominated by the inflow of water from the Atlantic through Fram Strait into the interior of the Arctic Basin, and its exit from the basin, also through Fram Strait. Estimates of the total heat loss within the basin vary widely because of insufficient direct measurements, uncertainty in the degree of recirculation of the warm Atlantic Water in northern Fram Strait, and large interannual variations. Values range

*Applied Physics Laboratory and School of Oceanography, College of Ocean and Fishery Sciences, University of Washington, Seattle, WA 98105, U.S.A.

from 68 TW (1 TW = 10^{12} W) (AAGAARD and GREISMAN, 1975) to 18 TW (RUDELS, 1978), with many values between (see HANZLICK, 1983). Within the Arctic Ocean the warm Atlantic Water is almost always separated from the surface by water with a temperature near freezing. In this paper we estimate the rate of heat loss from the Atlantic Water owing to diapycnal mixing across this temperature gradient. Only mixing due to the breaking and dissipation of internal gravity waves away from the immediate effect of the continental shelves is calculated.

This investigation is made possible by recent advances in parameterizing internal wave mixing (GREGG, 1987, 1989). OSBORN (1980) proposed that

$$K = \gamma \frac{\varepsilon}{N^2} \tag{1}$$

where K is the diapycnal diffusivity for density, ε is the dissipation rate of kinetic energy by molecular viscosity, N is the buoyancy frequency, and γ is a mixing efficiency, estimated at 0.2 (GREGG *et al.*, 1986; OAKEY, 1982). The direct measurement of ε, although routine with some researchers, is technically quite difficult. If, as is generally believed, internal waves supply the energy for mixing, ε should be related to the characteristics of the internal wave field. Such a relationship has been suggested (GREGG, 1989; HENYEY *et al.*, 1986). Combined with equation (1), it predicts

$$K = K_0 \langle S_{10}^4 / N^4 \rangle \tag{2}$$

where S_{10} is the shear including all vertical wave number components below 0.1 cpm, $\langle\rangle$ indicates an average over space or time, and $K_0 = 5 \times 10^{-6}\ \mathrm{m^2\ s^{-1}}$. The significance of (2) is that S_{10} and N are much easier to measure than ε. The GM spectrum corresponds to $\langle S_{10}^2/N^2 \rangle \approx 0.72$, and using equation (2) $K = 5 \times 10^{-6}\ \mathrm{m^2\ s^{-1}}$ (GREGG, 1989). For reference, if we assume a typical arctic vertical temperature gradient of 2×10^{-2}°C $\mathrm{m^{-1}}$, a uniform diapycnal diffusivity of about $0.5 \times 10^{-4}\ \mathrm{m^2\ s^{-1}}$ ($0.5\ \mathrm{cm^2\ s^{-1}}$) acting over the entire deep Arctic Basin ($10^{13}\ \mathrm{m^2}$) would produce a heat flux of 41 TW.

This paper describes the application of equation (2) to the Arctic Ocean. The variability of the internal wave field is examined using a collection of CTD and velocity profiles (Fig. 1) taken in Fram Strait during MIZEX 83 (JOHANNESSEN *et al.*, 1987) and north into the Arctic Ocean during cruise Arktis IV/3 of the R.V. *Polarstern* (ANDERSON *et al.*, 1989). Similar data from the Canada Basin (D'ASARO and MOREHEAD, 1991) are used to provide a deep arctic reference.

2. INSTRUMENTATION

Two types of instruments were used to provide the velocity data for this study. Free falling expendable Current Profilers (XCP) were deployed to make velocity profiles over a large geographical area during MIZEX 83 and *Polarstern* Arktis IV/3. The wire-lowered Arctic Profiling System (APS) was employed to obtain a time series of velocity profiles during MIZEX 83. The XCP data are used to determine the geographical variation in internal wave shear levels in these data; the APS data are used to depict conditions in one very energetic region over the Yermak Plateau.

2.1. *The XCP*

The basic XCP design is described by SANFORD *et al.* (1982). The device infers velocity, relative to a depth independent mean, by sensing the electric current induced in seawater

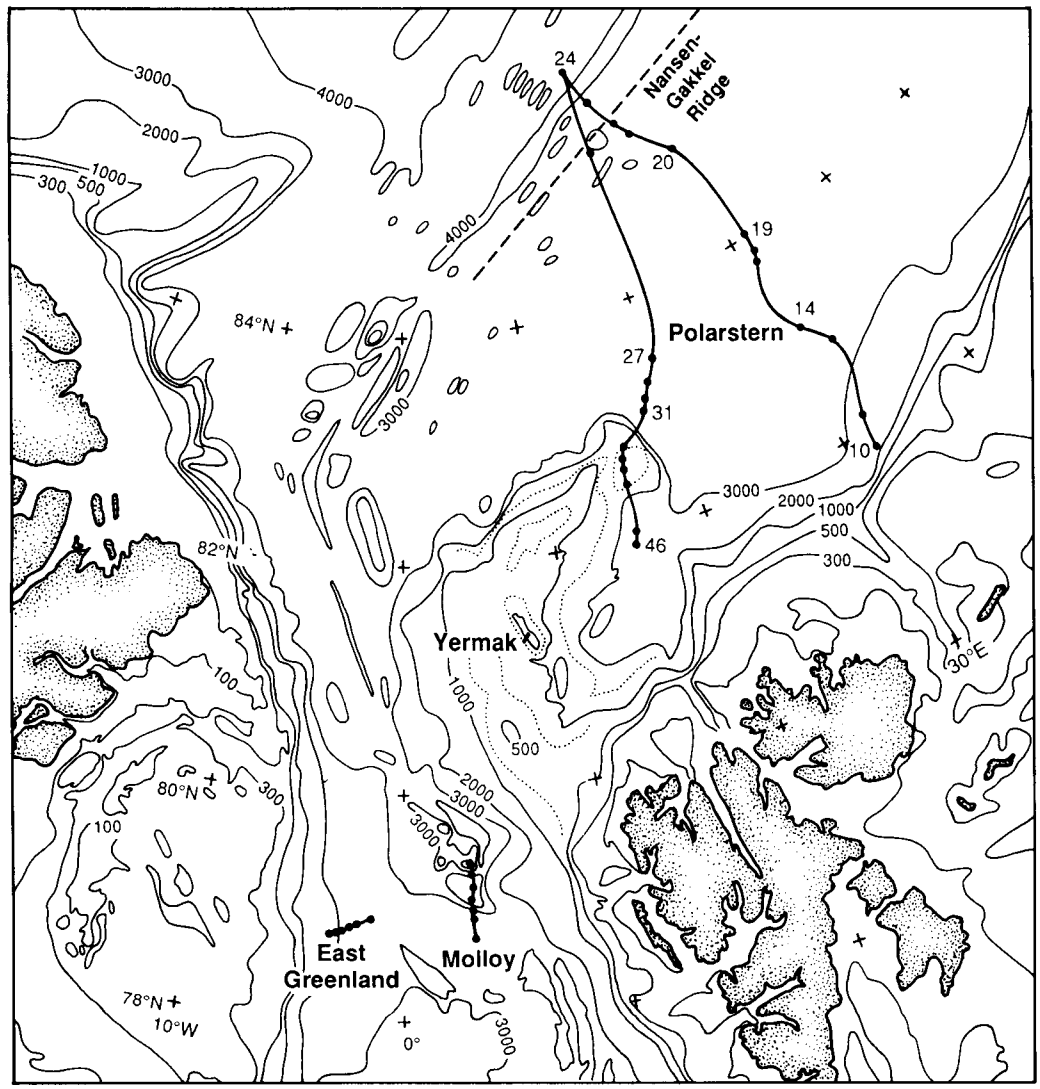

Fig. 1. Locations of XCP profiles used in this study. Profiles were taken on the northward and southward legs of the Arktis IV/3 cruise of the R.V. *Polarstern* and during MIZEX 83 in the East Greenland Current, over the Molloy Deep, and over the Yermak Plateau. The Nansen–Gakkel Ridge is poorly resolved on this map (PERRY and FLEMING, 1986). Its approximate axis is indicated by the dashed line. Contours are in meters.

by its motion through the earth's magnetic field. The expendable probe falls through the water at about 4.5 m s^{-1} and relays velocity, compass and temperature data to the surface along a pair of trailing, thin copper wires. After processing, the data have a vertical resolution of 5–10 m with a velocity error usually less than 0.01 m s^{-1}.

Two types of XCPs were employed. During MIZEX 83, a preproduction model was used identical to that described by SANFORD *et al.* (1982). Its maximum depth is about 950 m. Signals sent by wire from the probe to a shipboard recorder are amplified and

recorded on a small cassette recorder after the addition of a tone to compensate for tape wow. These are later replayed and processed. On *Polarstern*, production XCPs manufactured by Sippican Ocean Systems were used. These have a maximum depth of about 1500 m. Data are relayed from the probe to a free-drifting surface unit where they are transmitted by radio back to the ship. The demodulated RF signal from the probe is recorded, along with a constant tone, for later playback and analysis.

In both cruises, special procedures were used to launch XCPs well away from the ship and thus avoid contamination of the data by the ship's electric field. With the ship under way, the XCPs were thrown overboard, and an attached float released the probe after the ship had moved several shiplengths away. During MIZEX 83 the fuse delay described by SANFORD *et al.* (1982) was used. During the *Polarstern* cruise, the normal 40 s delay provided by Sippican was insufficient due to the ship's large size and its slow speed through the ice. The probes were therefore modified to provide a 160 s delay. When possible, XCPs were launched from ice floes well removed from the ship. For the *Polarstern* cruise, a small, water-resistant box containing a radio, receiver, amplifier, tone generator, and tape recorder was constructed. The XCP and the recording box were carried a few hundred meters from the ship, and the probe was launched into a lead or through a hole drilled in the ice.

Recorded telemetry data from the XCPs were replayed into digital receivers: the receiver described by SANFORD *et al.* (1982), for MIZEX 83; and a Sippican Mark-10, which is very similar, for *Polarstern*. Both sets of data were processed as described by SANFORD *et al.* (1982) to yield "raw" velocity and temperature estimates at a resolution of 0.6 and 0.3 m for the MIZEX 83 and *Polarstern* data, respectively.

2.2. *The APS*

The Arctic Profiling System employed is identical in principle to an earlier version described by MORISON (1978, 1980). It consists of a Sea-Bird CTD plus a triplet of small, ducted rotor velocity sensors measuring three orthogonal components of velocity relative to the instrument. A flux gate slaved, directional gyro and two accelerometers are used to determine the orientation of the instrument. Sensor data are transmitted up a single conductor, steel armored cable at a sample rate of 12 Hz and recorded directly on analog cassette tapes for redundancy and examination of fine scale structure. The data are also averaged over 1 s by the Sea-Bird deck unit and recorded on 5.25 inch floppy disks with an Apple microcomputer.

The APS was cycled to depths of up to 250 m using a winch mounted in a 3 × 1.5 m boat/sled called the Northern Light. This vehicle's small diesel engine powered the winch hydraulics and provided electrical power for the instrumentation. The winch raised and lowered the APS at a speed of 0.7 m s^{-1}. Casts were made at least once every 3 h. There were also sequences of continuous cycling for periods of 12 h or more. These were usually during periods of rapid ice motion. During the continuous runs, the profile interval was from 10 to 15 min depending on depth range.

2.3. *Comparison of XCP and APS velocity profiles*

The APS and XCPs were used simultaneously during days 187 to 189 of MIZEX 83. Figure 2 shows an XCP drop made at 2200Z on day 187 along with the interpolation of the

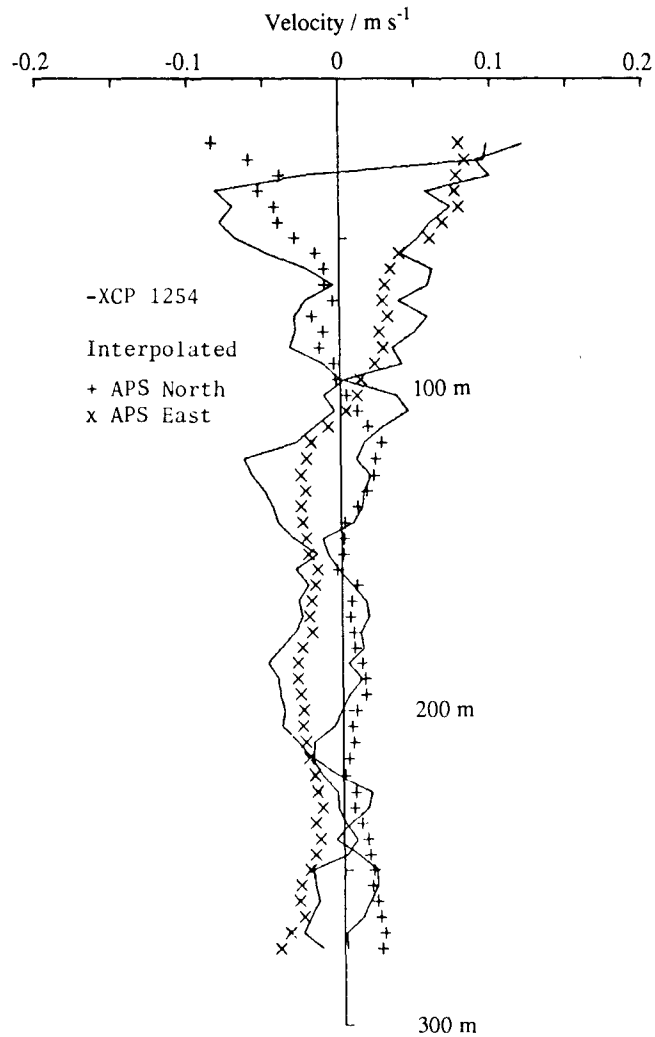

Fig. 2. Comparison of the velocity measured by XCP 1254 with the velocity measured by the APS and interpolated to the same time.

APS profiles just before and after the XCP drop. The profiles are similar in shape, but the APS data are smoother. The average vertical wave number spectra of six XCP drops and the spectra of APS profiles interpolated to the times of these drops are similar (Fig. 3). The APS spectrum lies below the XCP spectrum with the difference being less at low wave numbers. The coherence between the XCP and APS velocities (Fig. 4) is high only at the largest and smallest wave numbers; for wavelengths less than 100 m and greater than 15 m, the coherence between the two profilers is barely significant. Near 0.1 cpm, the transfer function is above one owing to the effect of averaging in the XCP processing. In the low frequency range where the coherence is high, the transfer function (Fig. 4) shows that the XCP velocities are only 10% higher than the APS velocities. The APS should therefore yield accurate measurements of the velocity field at low wave numbers. Its ability to

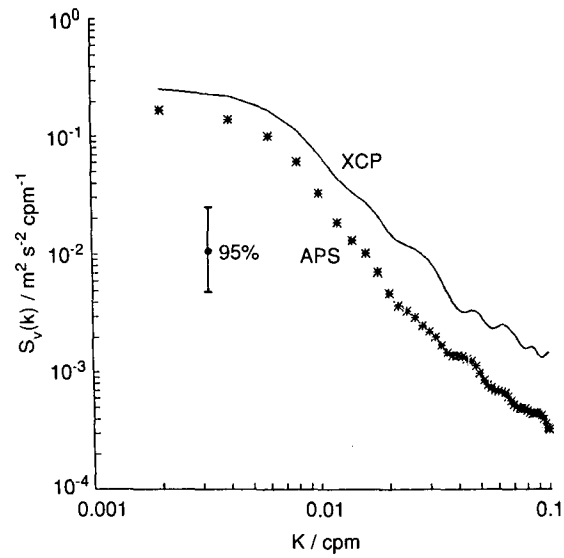

Fig. 3. Comparison of vertical wave number spectra of horizontal velocity from XCP and APS profiles made on day 187 during MIZEX 83. Since there are far more APS than XCP profiles, only the confidence limits for the XCP profiles are shown.

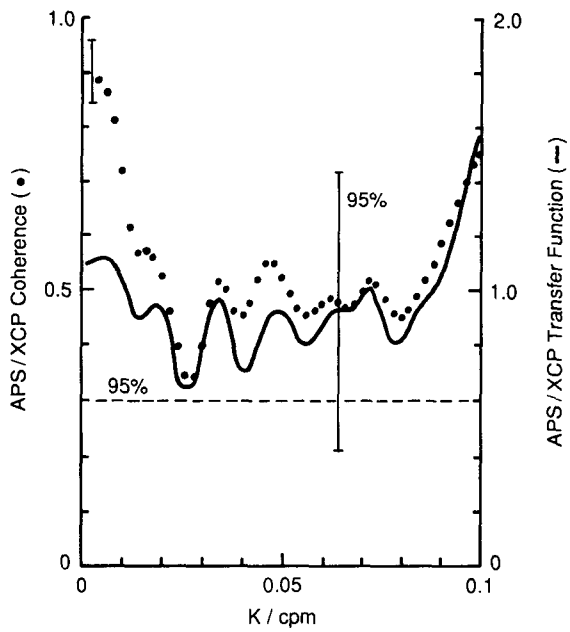

Fig. 4. Coherence (dots) and transfer function (line) between horizontal velocities from XCP and APS profiles during MIZEX 83 interpolated to the same time. The 95% level of no significance is shown for coherence, and 95% confidence limits are shown for the transfer function.

measure shear on a 10 m scale accurately is less certain, and APS data are not used for that purpose here.

The differences between velocities estimated from APS and XCP profiles can be explained by motion of the APS. At shallow depths, the APS agrees well with fixed current meters (MORISON, 1978, 1980). At the greater depths here, the APS probably reads low because it tends to move with the water as it descends. This effect is largest at medium wave numbers; at low wave numbers the cable effectively constrains the instrument, while at high wave numbers the inertia of the APS is great enough to keep the velocity errors small.

2.4. *CTD data*

For each XCP profile taken during the *Polarstern* cruise, T and S values from the one or two nearest hydrographic bottle stations (ANDERSON *et al.*, 1989) were linearly interpolated to a 10 m vertical grid and N^2 was computed as described by FOFONOFF and MILLARD (1983). In the depth range of 30–300 m, six to 15 bottles were used, with a mean of 11. For each XCP profile taken during MIZEX 83, CTD data from the APS, or from the ship's CTD (JOHANNESSEN *et al.*, 1984), were used. The buoyancy frequency was computed from a first difference of σ_t over a vertical separation such that σ_t differed by 0.01 between the points. Errors in the value of N computed in this way become significant below 400 m, so no CTD data below this depth were used.

2.5. *Error screening*

The XCP and CTD data were edited before estimating K. Data were retained only if the CTD data were sufficient to resolve N^2, if the XCP and CTD profiles of temperature agreed, and if the CTD data did not indicate a large horizontal gradient in N^2. The XCP velocity (u,v) and the shear components $(\partial u/\partial z, \partial v/\partial z)$, and their respective errors σ_V and σ_S, were estimated from the "raw" XCP data using a least squares linear regression over 10 m, half overlapping bins. We define $S^2 = (\partial u/\partial z)^2 + (\partial v/\partial z)^2$. The values of S^2_{10} and its error, $\sigma_{S^2_{10}}$, were estimated as $2.11S^2$ and $2.11\sigma_S^2$ respectively (GREGG, 1989). Note that this processing is exactly the same as that for XCP data in GREGG (1989).

Some N^2, S^2_{10} and K profiles representative of both high and low shear profiles are shown in Fig. 5. Note that in the low shear profiles (2017 and part of 2081) S^2_{10} is very close to $\sigma_{S^2_{10}}$, indicating that $\sigma_{S^2_{10}}$ is a good estimate of the noise level. Since $\sigma_{S^2_{10}}$ is nearly constant with depth, S^2_{10}/N^2 cannot be much smaller than $\sigma_{S^2_{10}}/N^2$, and can rise to large values for small N. This can be seen in the deeper parts of the sample profiles (Fig. 5). Accordingly, data points with $\sigma_{S^2_{10}}/N^2 > 1$ were discarded. Similarly, near the surface N^2 can become large and poorly defined (2017 and 2034 in Fig. 5). These data were also not used.

After editing, only profiles with more than 20 points were retained. The average number of points was 37 with a standard deviation of 11. Simulation of the statistical errors, with the assumption that the shear components are decorrelated in 10 m and that they are Gaussian, indicates that individual estimates of K made with 37 points will be within a factor of three of the true value.

Sample data in Fig. 5 illustrate the data quality and editing procedures. In each panel, profiles of N^2 and S^2_{10} are plotted on the right. The corresponding noise-corrected values of K that remain after editing are plotted on the left. In profiles 2017 and 2034, N^2 (heavy

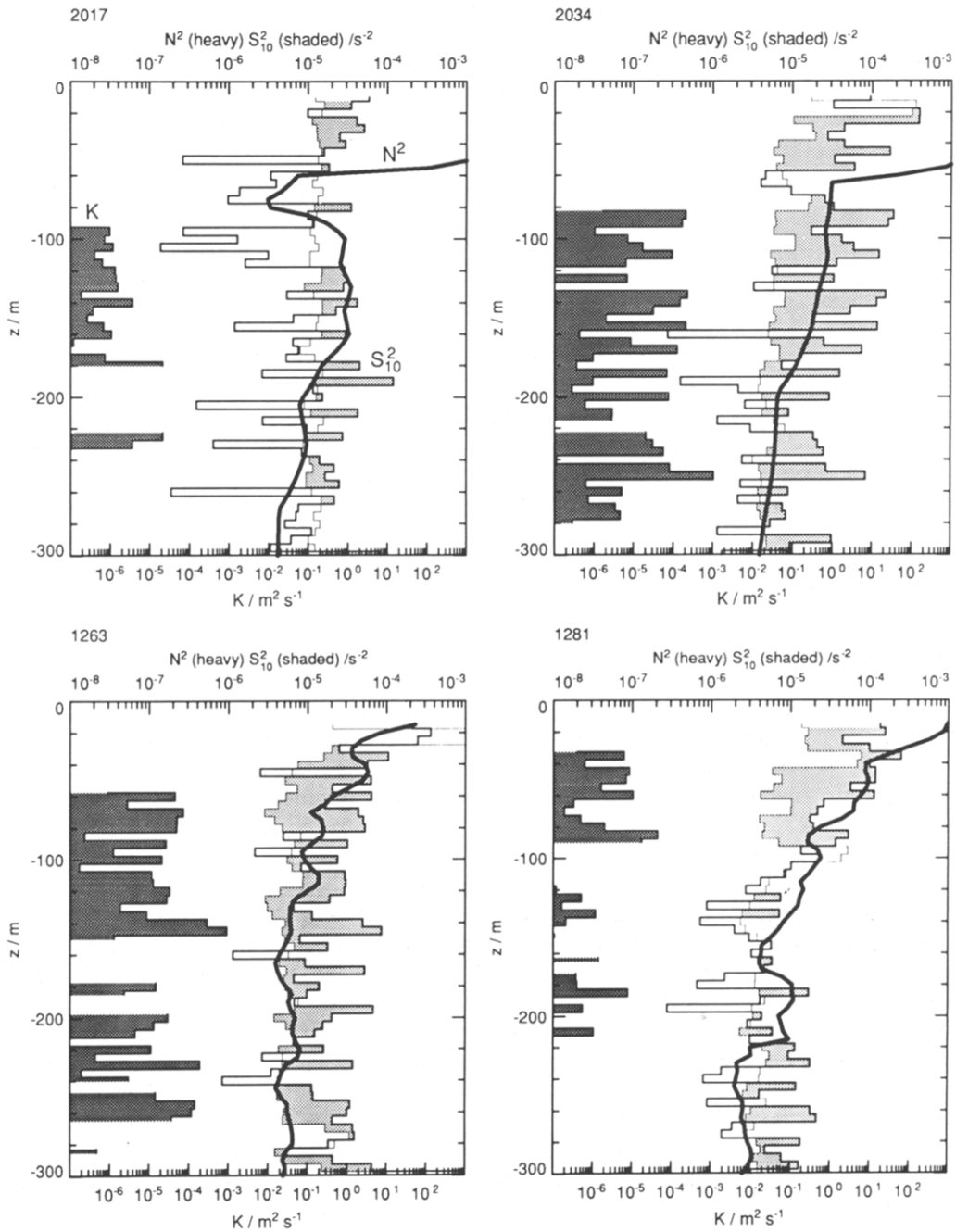

Fig. 5. Data from a low energy *Polarstern* profile (2017), a high energy *Polarstern* profile (2034), a high energy MIZEX 83 profile (1263), and a low energy MIZEX 83 profile (1281). Profiles of N^2 (heavy line), S^2_{10} (medium line), and $\sigma_{S^2_{10}}$ (light line) are plotted on right. Shading of S^2_{10} highlights the regions where $S^2_{10} > \sigma_{S^2_{10}}$. Diffusivity K, corrected for noise, is plotted left for data that pass the editing tests.

line) is large and poorly defined above about 50 m, so these data have been deleted. In the lower part of all profiles $\sigma_{S_{10}^2}/N^2 < F_{\min}$. Here K is excessively biased by the noise, and the data have been discarded.

3. DATA

3.1. Polarstern *Arkis* IV/3, 12 *July to* 16 *August* 1987

The locations of the XCP and hydrographic profiles from this cruise are shown in Fig. 1. On the northward leg, the ship's track crosses the Nansen Abyssal Plain and the Nansen–Gakkel Ridge, reaching 86°11′N at its northernmost point. The return track recrosses the Nansen Plain and then traverses the northeastern tip of the Yermak Plateau. Hydrographic and tracer data from this cruise are discussed by ANDERSON *et al.* (1989).

3.1.1. *Velocity features.* The XCP velocity profiles (Fig. 6a,b) show many interesting features. Over the Nansen Plain, the velocity is sometimes nearly uniform (e.g. profiles 2016, 2022, 2027, 2030, 2031). Other profiles show significant velocities both in the Atlantic Water layer (2010, 2011, 2013, 2029) and in the upper ocean (e.g. 2017, 2019, 2021). Although significant variability exists in the velocity field, it is generally difficult to determine whether it is due to high frequency or low frequency motions.

Profile 2029 (Figs 6b and 7) shows the characteristic signature of an anticyclonic submesoscale eddy (D'ASARO, 1988): strong rectilinear flow over a limited, subsurface depth interval with an associated anomaly in a conserved property—here the core of the Atlantic Water. Such eddies are typically 20 km across, and thus would not have been seen in adjacent profiles. This profile could be through such an eddy, or through a meander in the current of Atlantic Water that flows into the Eurasian Basin around the Yermak Plateau (AAGAARD *et al.*, 1987). The anticyclonic circulation is not definite, but is suggested by the thick central core; a cyclonic eddy would have a thin, "pinched" core.

A 0.5 m s^{-1}, surface intensified current (profile 2021, Fig. 6a) is found above the Nansen–Gakkel Ridge. The baroclinic flow is southwestward along the local axis of the ridge, consistent with AAGAARD's (1989) system of cyclonic, topographically trapped boundary currents in the Arctic Ocean. Assuming a steady flow and a horizontal extent of 10 km (about a Rossby radius, and also twice the distance to the closest XCP profile) the baroclinic transport of this current is only 0.5×10^6 m^3 s^{-1}. The previous profiles (2017, 2019) also show strong currents in this depth interval, although the next one (2022) does not.

Baroclinic currents of 0.15 m s^{-1} are seen near the bottom over the Yermak Plateau (Fig. 6b, profiles 2034–2041). The velocity varies dramatically between profiles, suggesting either a spatial scale of less than 10 km or strong temporal variability. Large tidal currents are known to exist on the flanks of the Yermak Plateau (HUNKINS, 1986).

3.1.2. *Shear levels.* Figures 8 and 9 plot estimates of N^2, $\langle S_{10}^2 \rangle$ (panel c), $\langle S_{10}^2 \rangle / N^2$ (panel b), and K (panel a) computed from individual XCP profiles. The bottom topography is shown in (d). Both instrumental noise and sampling errors can be significant here. In panel (b), $\sigma_{S_{10}^2}/N^2$, the estimated noise contribution to $\langle S_{10}^2 \rangle / N^2$, is indicated by the shaded region. The normalized shear level corrected for noise $\langle (S_{10}^2 - \sigma_{S_{10}^2}) \rangle / N^2$ (heavy dashed line) is also plotted. In panel (a), both corrected (heavy dashed) and uncorrected (heavy solid)

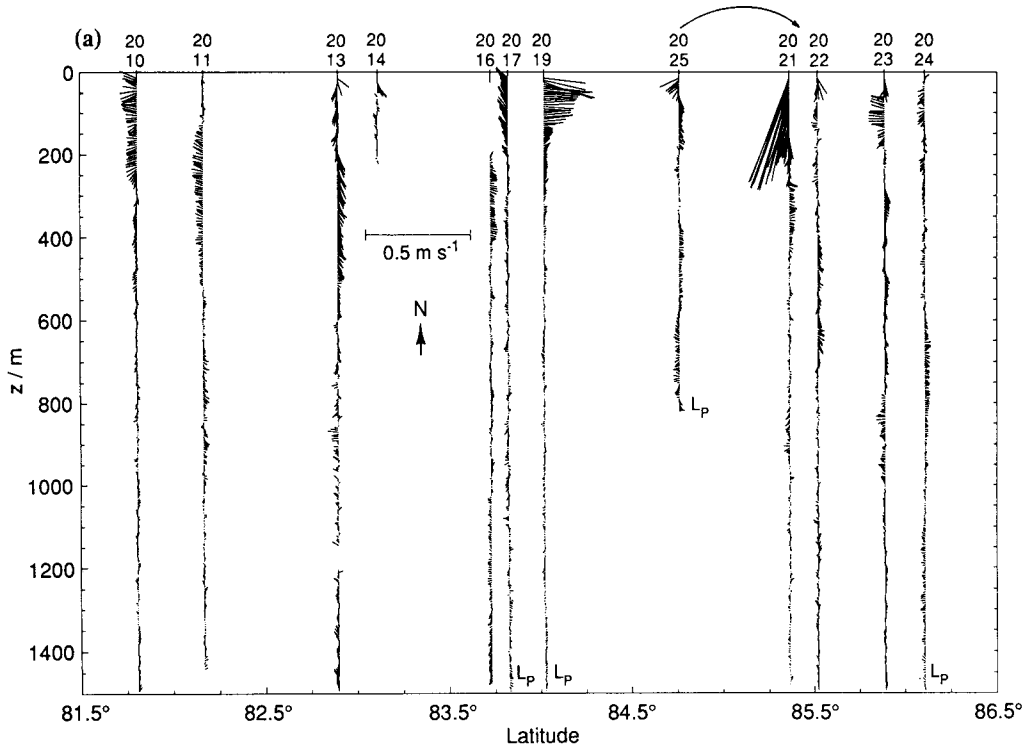
(a)
20 10
20 11
20 13
20 14
20 16
20 17
20 19
20 25
20 21
20 22
20 23
20 24
0
200
400
600
800
1000
1200
1400
z / m
0.5 m s-1
N
LP
81.5°
82.5°
83.5°
84.5°
85.5°
86.5°
Latitude

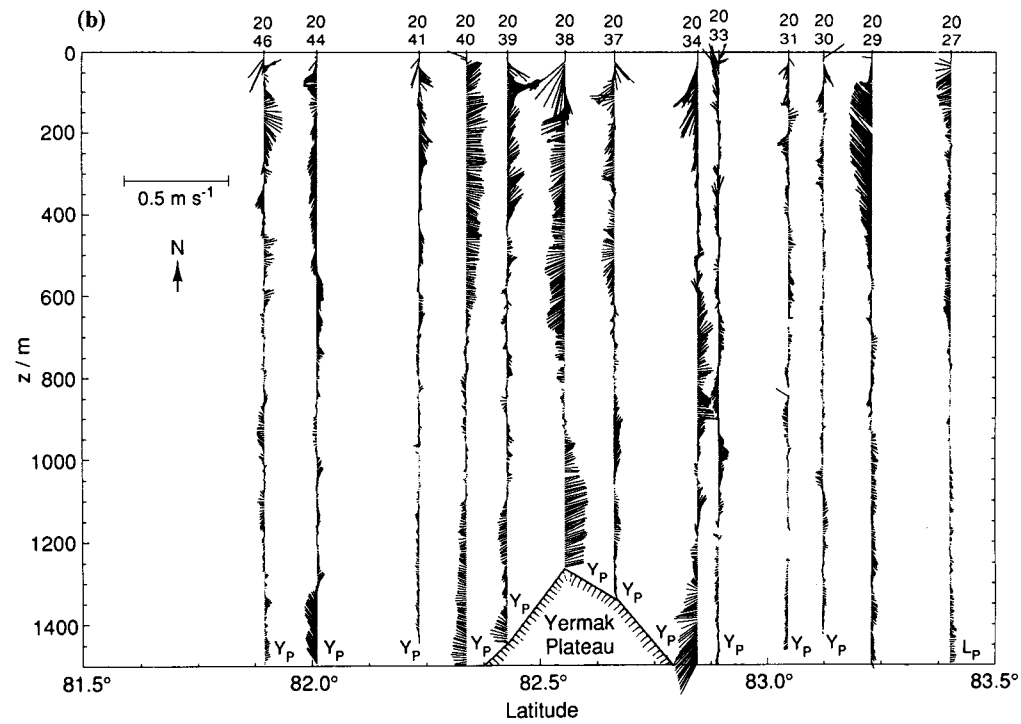
(b)
20 46
20 44
20 41
20 40
20 39
20 38
20 37
20 34
20 33
20 31
20 30
20 29
20 27
0
200
400
600
800
1000
1200
1400
z / m
0.5 m s-1
N
YP
Yermak
Plateau
LP
81.5°
82.0°
82.5°
83.0°
83.5°
Latitude

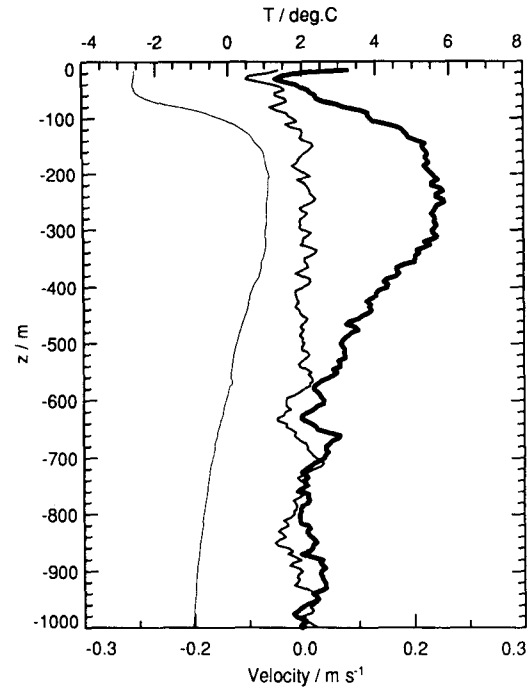

Fig. 7. XCP profile 2029. Velocity is rotated to show the jet centered on the warm core of Atlantic Water. Heavy velocity line is directed 45°W of north; light 45°E of north. The apparent large supercooling of the mixed layer relative to the freezing point is almost certainly due to calibration errors.

values of K are shown. Light lines in panels (a,b) indicate confidence limits computed from the 95% points of 500 bootstrap realizations (EFRON and GONG, 1983) of $\langle S_{10}^2 \rangle / N^2$ and K, both noise corrected (dashed) and uncorrected (solid).

Figures 8 and 9 show a dramatic variation in $\langle S_{10}^2 \rangle / N^2$ and K. Over the Nansen Abyssal Plain, the shear is close to the noise level of the XCP. Corrected for noise, $\langle S_{10}^2 \rangle / N^2$ varies from less than 0.2 to about 0.5; K varies between 1.5×10^{-6} and 7×10^{-6} m^2 s^{-1}. The larger values are comparable to GM; the smaller are closer to those found in the Beaufort Sea during AIWEX (D'ASARO and MOREHEAD, 1991). Over the Yermak Plateau, and in the limited data over the Nansen–Gakkel Ridge, the shear is far above the noise level of the XCP; $\langle S_{10}^2 \rangle / N^2$ is 2–4 and K is 0.3–2 $\times 10^{-4}$ m^2 s^{-1}. These values are about an order of magnitude above GM and comparable to the largest values in GREGG (1989).

3.2. *MIZEX* 83, 6–25 *July* 1983

XCP data, shown in Fig. 10, were taken in three regions of Fram Strait as shown in Fig. 1. A plan view of the upper ocean currents is shown in Fig. 11, and summary statistics are shown in Fig. 12.

Fig. 6. XCP profiles taken during *Polarstern* Arktis IV/3. Individual vectors give the current at each depth referenced to a 300–1600 m mean. Panel (a) shows profiles from northward leg; (b) from southward. Bottom topography determined from impacts of XCPs on the bottom is shown. The location of profile 2025 is indicated by the arrow. Symbols at the bottom of some profiles indicate that they were used in one of the spectra in Figs 15 and 16.

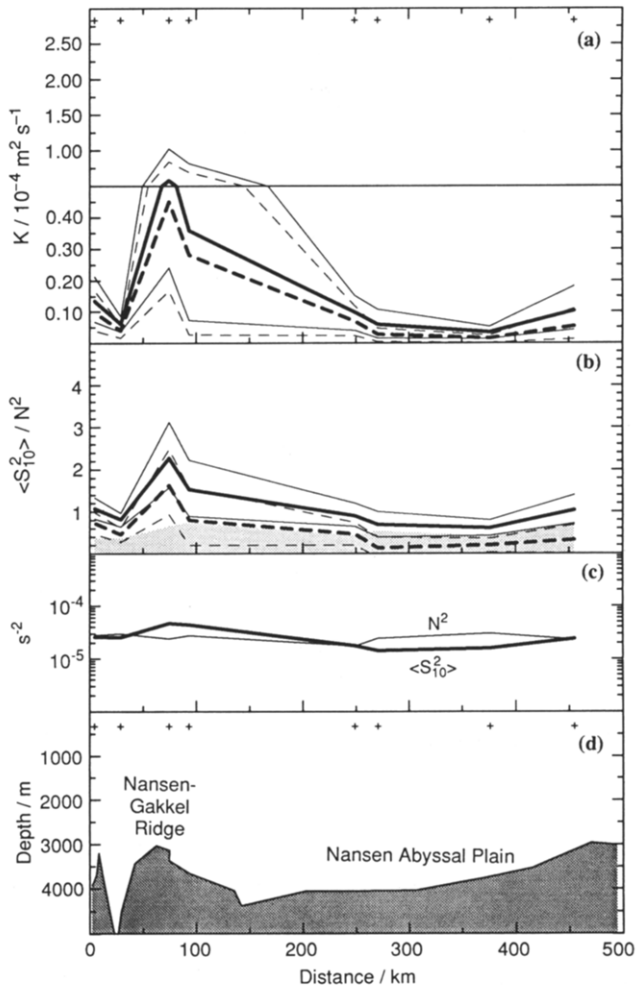

Fig. 8. Shear, stratification, and estimated diapycnal diffusivity for northward leg of *Polarstern* Arktis IV/3. For each XCP, indicated by +, average values of S^2_{10} and N^2 (panel c), their ratio (b), and the diapycnal diffusivity estimated by equation (2) (a) are shown. In panels (a),(b) dashed lines show values corrected for XCP noise; light lines give 95% confidence limits. The estimated XCP noise in S^2_{10} is indicated by the shading in (b). Bottom depth as measured by the ship's echo-sounder is indicated in (d). Bottom axis is great circle distance from 86.15°N, 22°E.

3.2.1. *East Greenland Current.* These profiles were made from drifting ice floes in the marginal ice zone of the East Greenland Current. The bottom topography is gently sloping. The velocity profiles (Figs 10 and 11) show the upper 300 m moving southward relative to deeper levels. The east–west shear is variable, but profiles 1278–1281 show a consistent eastward component at the surface. This pattern is probably due to the stations being on the eastern side of the East Greenland Current. The surface currents from profiles 1274 and 1275, combined with 1278–1281, suggest a cyclonic circulation with a radius of about 30 km. A similar circulation was deduced by Manley (1987), using nearly simultaneous CTD measurements, and identified as the "Polarbjorn eddy."

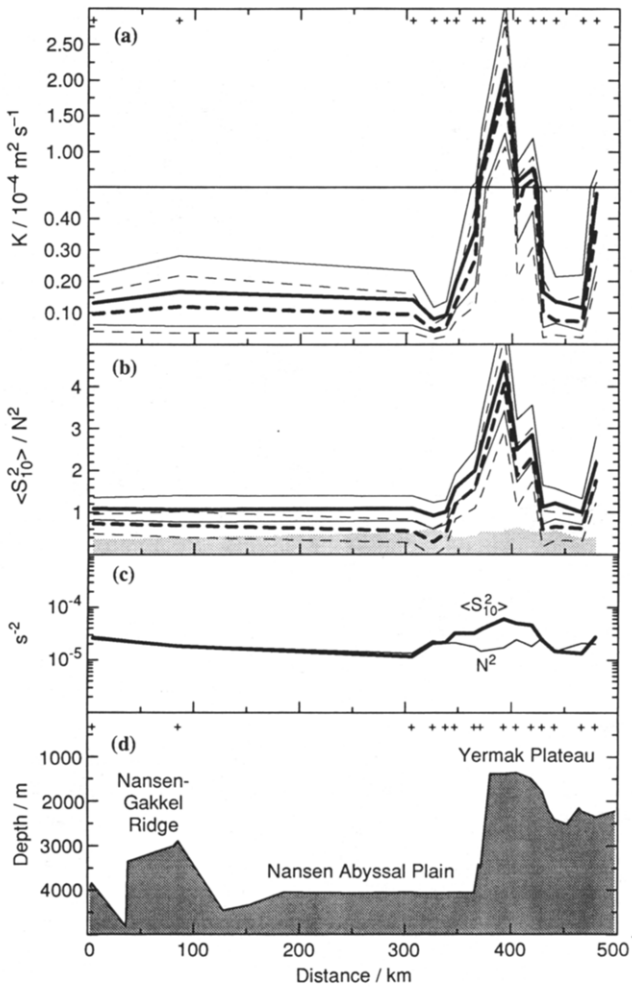

Fig. 9. Shear, stratification, and estimated diapycnal diffusivity for southward leg of *Polarstern* Arktis IV/3. See Fig. 8 for details.

Despite the large velocities, the shear levels (Fig. 12) are low, only slightly above the quietest *Polarstern* levels.

3.2.2. *Molloy Deep*. These profiles, made from the M.V. *Polarbjorn* in loose ice and open water, form a north–south section (Figs 1 and 11) over the Molloy Deep, the site of a large, persistent eddy (WADHAMS *et al.*, 1979; WADHAMS and SQUIRE, 1983; SMITH *et al.*, 1987; JOHANNESSEN *et al.*, 1987; BOURKE *et al.*, 1987). The near-surface currents (Figs 10b, 11) show considerable vertical structure. As presented in Fig. 10b, it is difficult to find obvious evidence of the Molloy Deep eddy. The XCP profiles were taken in two groups (1269–1272; 1283–1286) about a week apart. If the eddy is assumed to have moved 30 km northward during this time, however, a coherent pattern very similar to that described by BOURKE *et al.* (1987) emerges (Fig. 11). Rather than a single, isolated eddy, two westward flows and an eastward flow are found above 600 m depth.

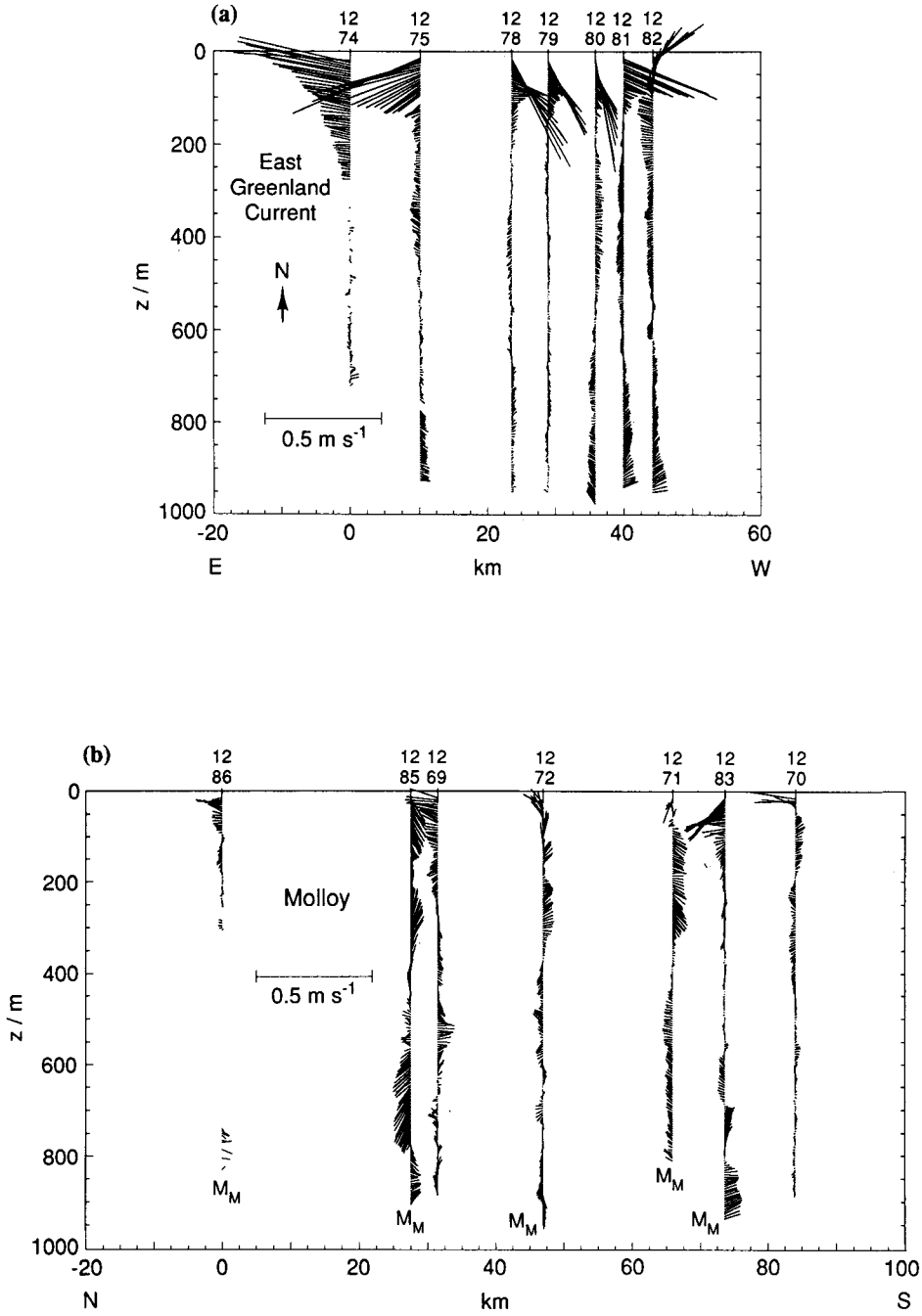

Fig. 10. XCP profiles from (a) East Greenland Current, (b) Molloy Deep, and (c) Yermak Plateau segments of MIZEX 83. Vectors give the current referenced to a 200 m to deepest data mean for (a) and to a 50 m to deepest data mean for (b),(c). Profiles from (a),(b) are plotted against distance from the first profile, while profiles from (c) are equally spaced. Bottom depths as measured by the XCP are plotted in (c). Symbols at the bottom of some profiles indicate that they were used in one of the spectra in Figs 15 and 16.

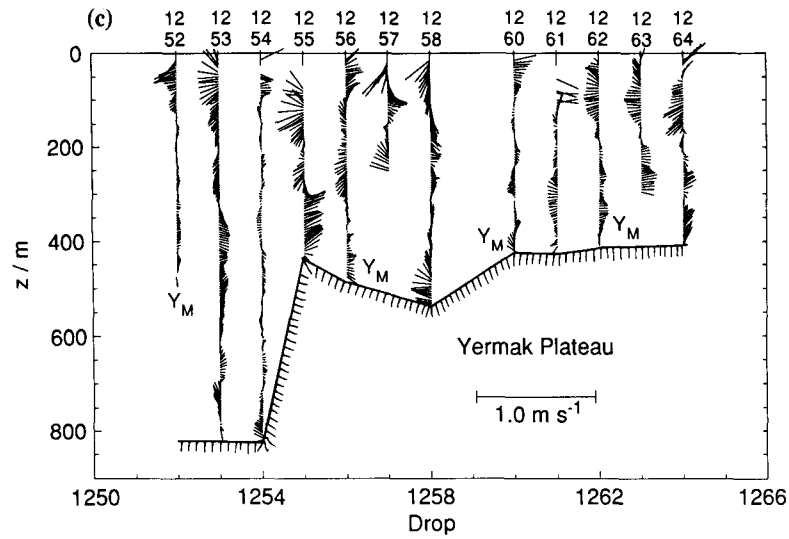

Fig. 10. *Continued.*

Independent of these details, this appears to be an area of strong horizontal velocity gradients. The shear levels (Fig. 12) peak over the Molloy Deep, with maximum values of $\langle S_{10}^2 \rangle / N^2$ reaching 1.5 and of K reaching 4×10^{-5} m^2 s^{-1}.

3.2.3. *Yermak Plateau.* XCP and APS data were taken from an ice floe that drifted up the side of an isolated elliptical seamount on the Yermak Plateau (Figs 1 and 13). The XCP profiles (Fig. 10c) suggest an elevated level of shear with K reaching 0.5×10^{-4} m^2 s^{-1} (Fig. 12).

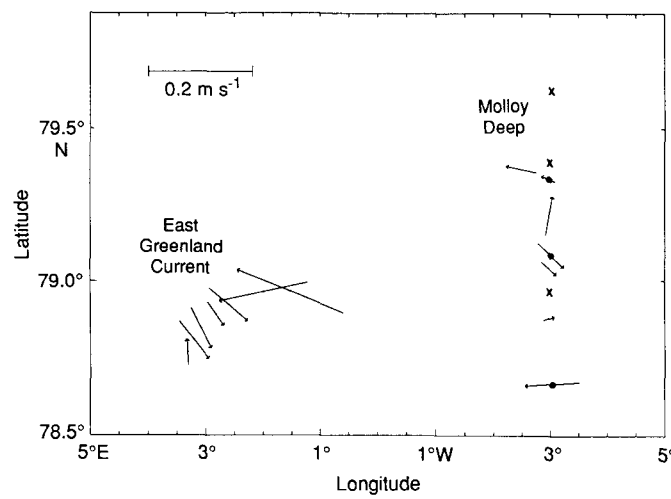

Fig. 11. Average 50–100 m velocities relative to a 500–950 m mean for XCP profiles in Fram Strait. Some of the profiles over the Molloy Deep have been shifted about 30 km south as discussed in the text. For these, an x indicates the true position, while a dot indicates the shifted position.

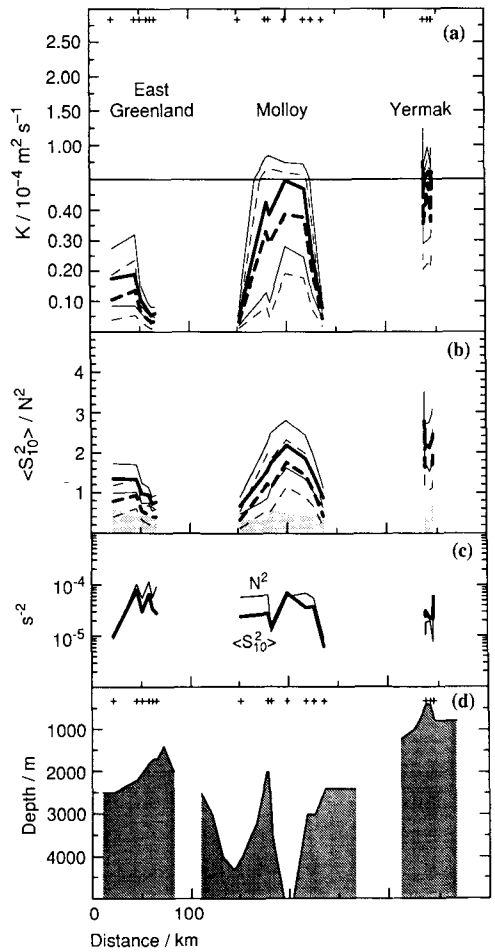

Fig. 12. Shear, stratification, and estimated diapycnal diffusivity for MIZEX 83 data. See Fig. 8 for details. Bottom depths are from PERRY and FLEMING (1986). Sections have the same orientation as in Fig. 10.

The APS data (Fig. 14) complement the XCP data by showing much larger shears on top of the seamount (days 187.5–189) than on the flanks (days 182–187). During the earlier period the measured currents are small, generally less than 0.05 m s^{-1}. The most notable feature is a wave packet on day 185 with a strong counterclockwise rotation of the velocity vector with depth. As the ice flow reaches the top of the seamount, the measured currents increase markedly (Fig. 14a) to about 0.2 m s^{-1}. The currents have a dominant near-inertial frequency, which at this latitude includes the semidiurnal tidal frequencies. This is shown in Fig. 14b, where the vectors have been inertially backrotated to day 182, 0000Z, strobing the data so that velocities rotating inertially appear constant in time. After day 187, a persistent pattern in the rotated data emerges. Vectors point to the left in the upper 100 m and to the right in the lower 150 m. This indicates the presence of strong, near-inertial frequency velocities with a vertical structure close to that of the first baroclinic

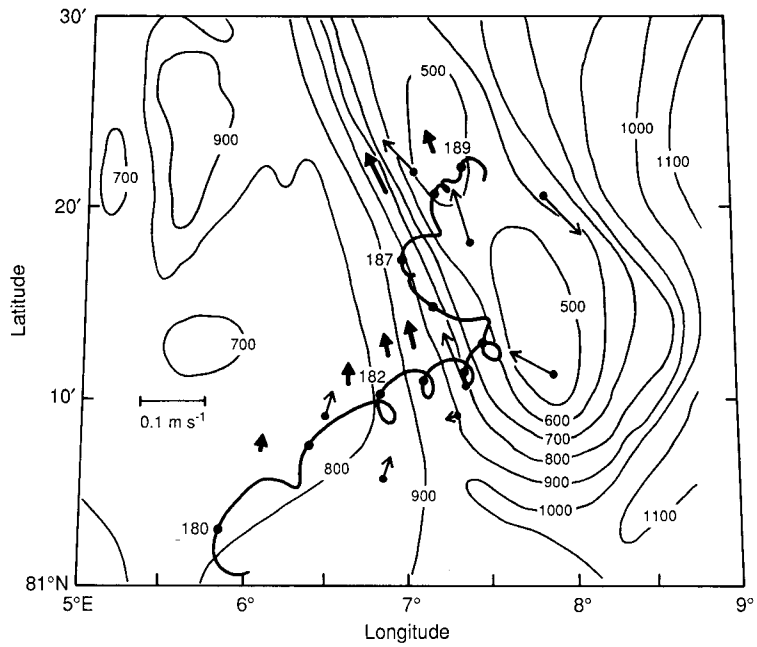

Fig. 13. Bottom topography and drift track for APS and XCP measurements in MIZEX 83; adapted from SANDVEN and JOHANNESSEN (1987). Dots on drift track show the start of each day. Arrows indicate selected low frequency currents from three ice-moored current meters described by JOHANNESSEN *et al.* (1984). Heavy arrows are 40 m depth; light arrows are 200 m. Currents are directed along topography indicating an anticyclonic relative vorticity above the seamount.

mode. There is some rotation of the velocity vectors counterclockwise with increasing depth, indicating an upward energy propagation if these motions are near-inertial frequency waves (LEAMAN and SANFORD, 1975).

Data from other MIZEX 83 investigators provide the context for these observations. A triangle of moorings surrounding the APS (JOHANNESSEN *et al.*, 1984) measure low frequency currents (36 h cutoff). At 200 m (Fig. 13) these currents closely follow the topographic contours. They are strongest (0.10–0.12 m s^{-1}) where the topographic slope is largest. Thus the region of enhanced near-inertial velocities is also a region of anomalous relative vorticity $\zeta \approx -0.15f$ (anticyclonic), centered approximately on the seamount.

The ice motion (Fig. 13) changes from an eastward drift with dominantly diurnal oscillations before day 185, to a northward drift with dominantly near-inertial oscillations (MCPHEE, 1984) on days 185–187, and finally to an eastward drift on days 188–189. These changes in ice drift appear to be correlated with changes in the wind (SANDVEN and JOHANNESSEN, 1987). The current meter moorings all show a large increase in near-inertial frequency currents starting on about day 186, coinciding approximately with the first wind shift. The APS data (Fig. 14) show the enhanced near-inertial shear beginning at about the second wind shift. Thus the region of enhanced near-inertial shear over the seamount also correlates with wind changes.

The enhanced shear levels in MIZEX 83 appear to be due to upward propagating, near-inertial frequency waves. The local oceanographic conditions are complicated, with

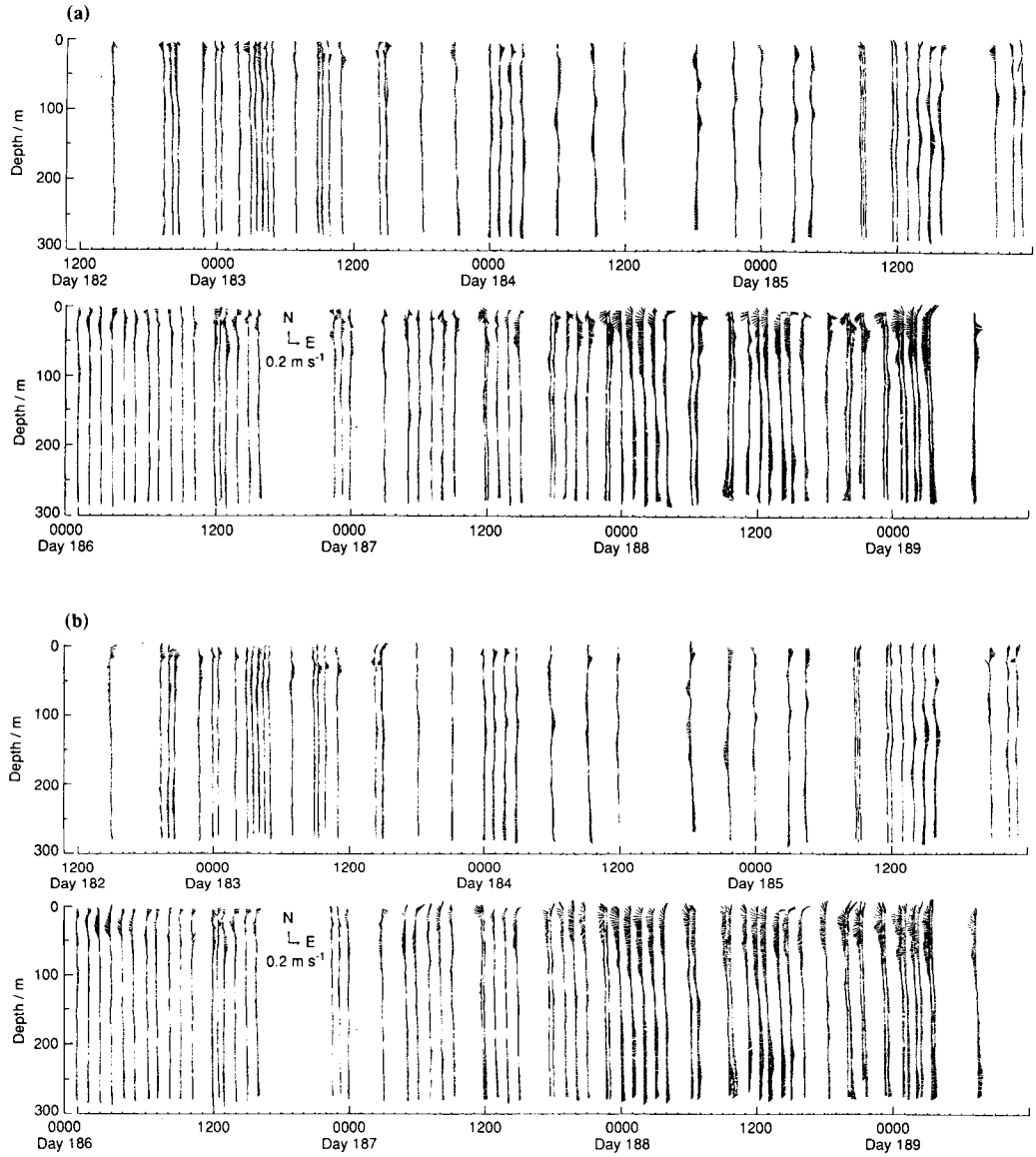

Fig. 14. APS velocity profiles for Yermak Plateau drift from MIZEX 83. Panel (a) gives measured velocities relative to the ice. Panel (b) gives same velocities backrotated at the local inertial frequency to 0000Z, day 182, to show the strong inertial frequency component.

simultaneous variations in topography, relative vorticity, and wind forcing, so the reasons for the high energy levels are not immediately obvious. Nevertheless, the data do constrain the possibilities.

First, the relative vorticity is sufficiently high ($-0.15f$) to allow the trapping of near-inertial waves. In the presence of relative vorticity, free internal waves with frequencies between N and $f + \frac{1}{2}\zeta$ can exist, in contrast to the usual constraints of N to f (KUNZE, 1985). Thus waves with frequencies between f and about $0.85f$ would be trapped within the

barotropic vorticity field centered on the seamount. This may account for the highly localized patch of near-inertial energy.

Second, the near-inertial oscillations of the ice that appear on day 185 and are apparently generated by the wind are too weak to be the sole cause of the near-inertial shear observed on days 187–189. The 5 m winds during this period were less than 5 m s^{-1} at the mooring locations (JOHANNESSEN and FARRELLY, 1984), but were quite variable. The maximum wind stress is thus about $\tau = \rho_A C_D U_A^2$; with $C_D = 3 \times 10^{-3}$ (GUEST and DAVIDSON, 1987), $\rho_A = 1.2\,\mathrm{kg\,m^{-3}}$, and $U_A = 5\,\mathrm{m\,s^{-1}}$, $\tau = 0.1\,\mathrm{N\,m^{-2}}$. Late on day 185, the wind shifts and the stress magnitude drops rapidly. This should generate inertial currents of magnitude

$$U_{\mathrm{wind}} = \frac{\tau_{\max}}{\rho f H} \tag{3}$$

(D'ASARO, 1985) and a total energy input of

$$E_{\mathrm{wind}} = \tfrac{1}{2}\rho H U_{\mathrm{wind}}^2 \tag{4}$$

for a slab of thickness H. Usually, H is set to the mixed layer depth. In MIZEX 83, however, the APS data show that strong stratification exists to the bottom of the ice. If we assume a combined ice thickness and boundary layer thickness of 2 m, $U_I = 0.34\,\mathrm{m\,s^{-1}}$ and $E_{\mathrm{wind}} = 184\,\mathrm{J\,m^{-2}}$. The observed near-inertial ice oscillations are considerably less than this, which suggests that this is an overestimate. Our choice of H could easily be too small, and the wind stress drop could easily be slower and smaller than assumed in (3). Regardless, the observed near-inertial currents have a magnitude U_I of about 0.1 m s^{-1} and an approximately sinusoidal structure that extends to a depth $D > 300$ m. Their energy is

$$E_I > \rho D \frac{U_I^2}{4} \tag{5}$$

or 768 J m^{-2}. This is about four times larger than E_{wind} estimated above. The observed inertial currents could be due either to the cumulative effect of several wind forcing events or to a single event locally enchanced by the vorticity field. The polarization of the waves, however, suggests upward propagation and a source other than surface forcing.

Third, tides are an attractive source for the enhanced near-inertial energy. Internal tides are effectively generated by the flow of the barotropic tide over topography. This has been documented by numerous observations (LEVINE, 1983; LEVINE *et al.*, 1983; PINGREE and NEW, 1989) and has a strong theoretical basis (WUNSCH, 1975). Pressure data taken by one of us (J.M.) on the Spitsbergen shelf show that M_2 is the strongest semidiurnal component in this region. More importantly, M_2 is subinertial ($0.964f$) at this latitude, but above the low frequency cutoff ($\approx 0.85f$) when the relative vorticity of the flow is included. We can envision a baroclinic internal tide that is generated on the seamount by the barotropic tide and trapped to the seamount by the barotropic vorticity field. Or, the baroclinic tide could be trapped near its generation site by the topography alone (WUNSCH, 1975; WUNSCH and HENDRY, 1972; BRINK, 1989). Tidal generation is also consistent with the upward energy propagation suggested by the wave polarization.

3.3. *Vertical wave number spectra*

Vertical wave number spectra of horizontal velocity profiles, WKB stretched according to the scheme of LEAMAN and SANFORD (1975), are shown in Fig. 15a–c for various groups

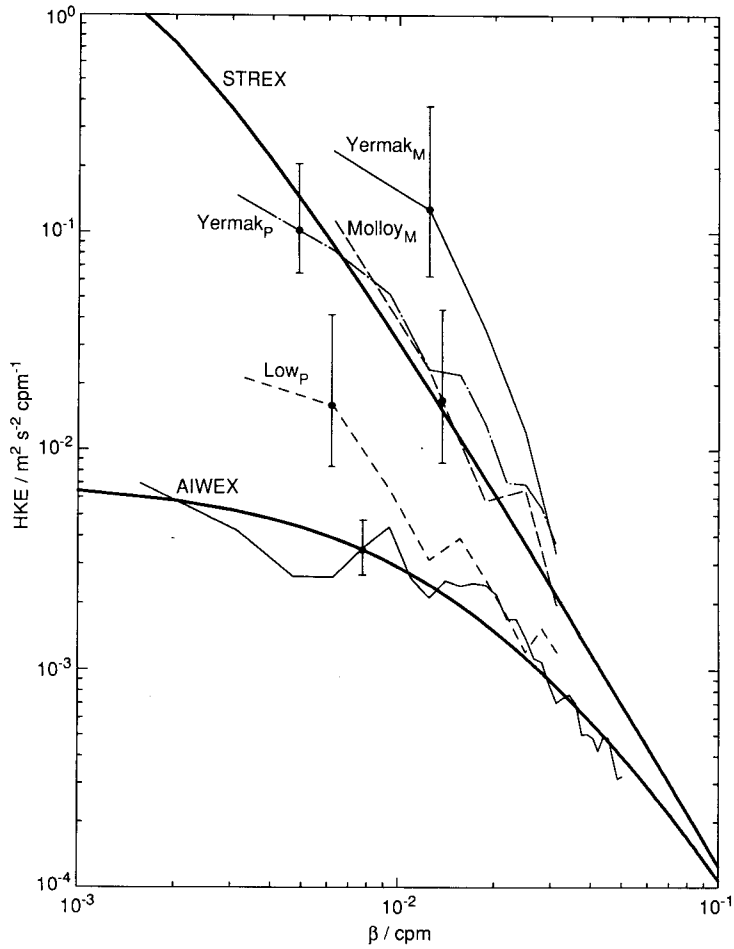

Fig. 15. Vertical wave number spectra of horizontal kinetic energy per unit mass for selected groups of XCP profiles. Heavy lines indicate approximate spectral levels for the AIWEX and STREX measurements. Profiles used in each group are indicated by labels on Figs 6 and 10 (code: L_P = Low, M_M = Molloy, Y_P = Yermak Plateau from *Polarstern*, Y_M = Yermak Plateau from MIZEX 83).

of XCP profiles. Individual velocity estimates for which $\sigma_v < 0.02$ m s^{-1} were removed, and the resulting gaps were filled by linear interpolation. Data were stretched starting at the deeper of 50 m or the depth of the first good data using the local N profile and a reference N of 5.23×10^{-3} s^{-1} (3 cph), and windowed using a 100% cosine taper. Periodograms from all the profiles in each group were averaged; no band averaging was done. Spectral values for stretched vertical wave numbers $\beta > 3 \times 10^{-2}$ cpm are not shown, because the data appear to reach a noise floor for higher wave numbers. Profiles used in these spectra are marked in Figs 6 and 10.

Heavy lines in Figs 15 and 16 provide the approximate limits of previously observed spectra. Each is an approximate fit of GM75 (GARRETT and MUNK, 1975). The upper line fits the STREX data (D'ASARO, 1984), which were taken during a period of storms in the northeastern Pacific Ocean ($j_* = 3$ and $E_0 = 10^{-4}$, using the notation of GARRETT and

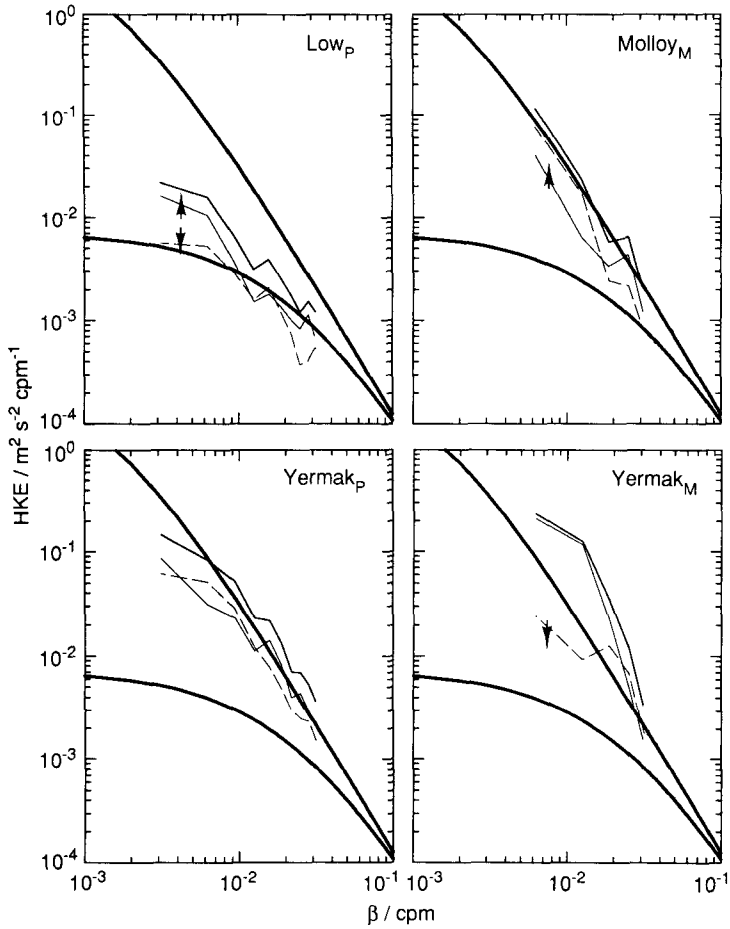

Fig. 16. Vertical wave number spectra of horizontal kinetic energy (heavy), clockwise (dashed; arrow down), and anticlockwise (light; arrow up) rotating energy for selected groups of XCP profiles.

MUNK, 1975). This spectrum is representative of the higher range of GM levels. The lower line ($j_* = 60$, $E_0 = 1.57 \times 10^{-6}$) fits the AIWEX data (D'ASARO and MOREHEAD, 1991).

Figure 15 shows average spectra from several groups of XCP profiles. The levels show a progression from levels far below GM during AIWEX, through somewhat higher levels for the quietest profiles taken on the *Polarstern* cruise ("Low$_P$"), to levels comparable to GM for profiles taken over the Molloy Deep during MIZEX 83 ("Molloy$_M$") and over the Yermak Plateau on the *Polarstern* cruise ("Yermak$_P$"). Finally, the profiles taken over the Yermak Plateau during MIZEX 83 ("Yermak$_M$") are well above GM. These profiles illustrate the transition of the internal wave climate from the low midbasin values to levels at and above GM, in parts of Fram Strait. East Greenland Current spectra from MIZEX 83 are not shown because of the obvious noninternal wave shear in the upper ocean. Clearly, the spectra shown here do not collapse to a universal curve. The spread, however, is less at high wave numbers than low, perhaps indicating a tendency toward universality at small scales.

It is worth noting that although the quietest profiles here are about three times more energetic than the AIWEX profiles in a WKB sense, this is mostly due to N being about three times smaller here than at AIWEX. In absolute terms, the energies over the Nansen Abyssal Plain are very similar to those found during AIWEX.

Figure 16 shows clockwise and anticlockwise spectra for the same data. There are only marginally significant differences between the clockwise and anticlockwise components except for the Yermak Plateau data from MIZEX 83. Here, the spectra are dominated by low mode, anticlockwise polarized motions corresponding to downward phase propagation for near-inertial waves and thus upward energy propagation. This is consistent with the APS data in Fig. 14 and a similar spectral analysis of APS data.

4. WHY DOES THE SHEAR LEVEL VARY?

A striking result in these data is the strong correlation between normalized shear levels and topography. PLEUDEMANN (personal communication, 1989) also sees increases in shear over the Yermak Plateau compared with the Nansen Abyssal Plain, while PADMAN and DILLON (1991) see an increase in both internal wave activity and turbulent kinetic energy dissipation along the western slope of Yermak Plateau. These variations are remarkable compared with the far more uniform shear levels found in mid-latitudes.

LEVINE *et al.* (1985, 1987) give several reasons why the internal wave energy should be low in the Arctic: The ice cover is an efficient absorber of internal waves (MORISON *et al.*, 1985). It also may absorb some of the atmospheric stress, particularly at small spatial scales, and thus inhibit the generation of internal waves by the atmosphere. Finally, Arctic Ocean tides are generally weak, so tidal generation of internal waves may be small. These perhaps explain the low shear levels found over the plains. But why are the levels so much higher on rougher topography?

One possible answer is that tides acting on rough topography are the major source of internal waves in the Arctic. This effect would be absent over the plains, where strong damping by the ice cover would rapidly attenuate the waves. The existing data are consistent with this idea. The MIZEX 83 data suggest M_2 tidal forcing as a likely source of the enhanced shear. The highest shears found on the *Polarstern* cruise occurred on the outer edge of the Yermak Plateau, an area known to have resonantly enhanced diurnal tides (HUNKINS, 1986; BRINK, 1989). Similarly, PADMAN and DILLON (1991) find their highest turbulent kinetic energy dissipations on the outer edge of the Yermak Plateau in association with packets of high frequency waves apparently excited by this diurnal tide. SANDVEN and JOHANNESSEN (1987) found similar packets during MIZEX 83. Although the diurnal barotropic tide is probably strong only over the Yermak Plateau, the barotropic M_2 tide produces 0.02–0.10 m s^{-1} currents over most of the Arctic Ocean's deep water (KOWALIK and UNTERSTEINER, 1978). These currents should be capable of generating internal waves wherever suitable topography exists.

5. IMPLICATIONS FOR THE ARCTIC HEAT BUDGET

These measurements, and those of D'ASARO and MOREHEAD (1991), suggest that shear levels in the Arctic Ocean are very low over the plains, leading to minute values of K there. In contrast, K reaches 1.8×10^{-4} m^2 s^{-1} over the flank of the Yermak Plateau, as calculated here. Using the local vertical temperature gradient of about 3°C per 100 m between the Atlantic Water and cold halocline, this corresponds to 22 W m^{-2}, close to PADMAN and DILLON's (1991) estimated heat flux of 27 W m^{-2} in a nearby location. We

suspect that these values are anomalously large due to diurnal tides on the flanks of the Yermak Plateau. More typical are values of $K \approx 5 \times 10^{-5}$ m^2 s^{-1} which occur in four other regions of "rough" topography sampled (Molloy, top of Yermak Plateau in MIZEX 83 and in *Polarstern*, Nansen–Gakkel Ridge). With vertical temperature gradients of 1–2°C per 100 m, the associated diapycnal heat flux is 2–4 W m^{-2}. We suggest that these may be typical heat fluxes away from the abyssal plains. Roughly 30% of the deep Arctic Basin is not abyssal plain, 3×10^{12} m^2, yielding a total heat flux of 6–12 TW.

What are the implications of this for the overall Arctic Ocean heat budget? Estimates of the total heat loss in the Arctic Ocean range from 18 TW (RUDELS, 1987) to 68 TW (AAGAARD and GREISMAN, 1975). We know that much of this heat is lost just north of Fram Strait. This is seen, for example, in the maps of TRESHNIKOV and BARANOV (1972) and COACHMAN and BARNES (1963)—which show a rapid decrease in the temperature of the Atlantic Water eastward away from Fram Strait. More quantitatively, UNTERSTEINER (1988) estimates that 17 TW is lost to melting ice, and MARTIN and CAVALIERI (1989) estimate about 1–2 TW are lost in island polynyas, for a total of 19 TW heat loss in this area. This leaves −1 to 49 TW to be lost in the rest of the basin. The negative value is obtained using RUDELS' (1987) heat flux estimate, which indicates that it is too low. Averaging 49 TW (AAGAARD and GREISMAN, 1975) over the 10^{13} m^2 area of the Arctic Ocean, the vertical heat flux is 4.9 W m^{-2}. A rough lower limit on the diapycnal heat flux is possible by assuming that all the cooling of Atlantic Water near Fram Strait seen in the maps of COACHMAN and BARNES (1963) is due to melting of ice. Using Untersteiner's estimate of 17 TW and a guess from the maps that this accounts for 80% of the cooling, the remaining 20% amounts to 5 TW, or 0.5 W m^{-1}. We conclude that the large scale heat balance probably requires a loss of 5–49 TW (0.5–5 W m^{-2}) in the Arctic Ocean. The large range reflects our ignorance.

The diapycnal heat fluxes due to internal waves (6–12 TW) barely overlap the possible range of heat fluxes required by the large scale heat budget estimates. Internal wave mixing can therefore not be ignored as a heat transport mechanism in the Arctic Ocean, but it is probably not the most important one. This conclusion is subject to direct tests of the parameterization (2) in the arctic environment. The large spatial variability observed suggests that internal wave mixing may be important to the heat balance of local regions. PADMAN and DILLON (1991) attempt to demonstrate this for the flow of Atlantic Water past the Yermak Plateau. The variability also indicates that diapycnal mixing may be weak over large regions of the Arctic Ocean. KILLWORTH and SMITH (1984) estimate K at about 10^{-6} m^2 s^{-1} for the Canada Basin based on the distribution and inputs of temperature and salinity. WALLACE *et al.* (1987) include the distribution of chlorofluoromethane and oxygen and estimate 2×10^{-6} m^2 s^{-1}. These values are an order of magnitude below our values for "rough" topography, even though the Canada Basin has a significant area that is not abyssal plain. Attempts to make accurate estimates of the total heat flux due to internal wave mixing will have to contend with this spatial variability. Two likely approaches are high resolution modeling of the effects of topography or high resolution sampling of mixing rates.

6. SUMMARY

Observations of shear in the Eastern Arctic, combined with AIWEX observations (D'ASARO and MOREHEAD, 1991), suggest an arctic internal wave field that is highly variable.

(i) Shear levels are lowest over the abyssal plains, but are comparable to mid-latitude values near rougher topography in Fram Strait. High levels over the Nansen–Gakkel Ridge and low levels over smooth topography in Fram Strait suggest that topography, not distance into the pack ice, is the most important factor.

(ii) Nearly two orders of magnitude variation in $\langle S_{10}^4 \rangle N^{-4}$ are found. This corresponds, by (1) and (2) (GREGG, 1989), to variations in the internal wave induced diapycnal diffusivity from near molecular to 2×10^{-4} m^2 s^{-1}.

(iii) The WKB-scaled vertical wave number spectra of horizontal velocity are comparable to those from mid-latitudes over "rough" topography, but are less energetic and whiter over the abyssal plains.

(iv) An internal wave source associated with rough topography and a nearby sink to limit wave propagation is implicated. We suggest a source driven by the barotropic tides and a sink in the ice–water frictional layer.

(v) Extrapolation of these observations to the entire Arctic Basin suggests that internal wave mixing could be a major heat transfer mechanism, but probably not the most important one. The large spatial variability of the mixing rate and the unknown accuracy of (2) in the Arctic are the major sources of uncertainty in estimating the heat flux.

Acknowledgements—The *Polarstern* XCP data shown here were gathered by Pat McKeown with the assistance of Jim Swift at the invitation of the Alfred Wegener Institute. Tom Sanford provided the equipment for making the MIZEX 83 XCP measurements. This work was supported by contract N00014-87-K-0004 from the Office of Naval Research. This paper is dedicated to the late Richard Trowbridge for his help, encouragement, and good advice to both of us during our early scientific careers. School of Oceanography Contribution Number 1847.

REFERENCES

AAGAARD K. (1989) A synthesis of the Arctic Ocean circulation. *Rapports et Proces-Verbaux des Reunions. Conseil Permanent International pour l'Exploration de la Mer*, **188**, 11–22.

AAGAARD K. and P. GREISMAN (1975) Toward new mass and heat budgets for the Arctic Ocean. *Journal of Geophysical Research*, **80**, 3821–3827.

AAGAARD K., A. FOLDVICK and S. R. HILLMAN (1987) The West Spitsbergen Current: disposition and water mass transformation. *Journal of Geophysical Research*, **92**, 3778–3784.

ANDERSON L. G., E. P. JONES, K. P. KOLTERMAN, P. SCHLOSSER, J. H. SWIFT and D. W. R. WALLACE (1989) The first oceanographic section across the Nansen Basin in the Arctic Ocean. *Deep-Sea Research*, **36**, 475–482.

BOURKE R. H., M. D. TUNNICLIFFE, J. L. NEWTON, R. G. PAQUETTE and T. O. MANLEY (1987) Eddy near the Molloy Deep revisited. *Journal of Geophysical Research*, **92**, 6773–6776.

BRINK K. H. (1989) The effect of stratification on seamount-trapped waves. *Deep-Sea Research*, **36**, 825–844.

COACHMAN L. K. and C. A. BARNES (1963) The movement of Atlantic Water in the Arctic Ocean. *Arctic*, **16**, 8–16.

D'ASARO E. A. (1984) Wind forced internal waves in the North Pacific and Sargasso Sea. *Journal of Physical Oceanography*, **14**, 781–794.

D'ASARO E. A. (1985) The energy flux from the wind to near-inertial motions in the surface mixed layer. *Journal of Physical Oceanography*, **15**, 1043–1059.

D'ASARO E. A. (1988) Observations of small eddies in the Beaufort Sea. *Journal of Geophysical Research*, **93**, 6669–6684.

D'ASARO E. A. and M. D. MOREHEAD (1991) Internal waves and velocity fine structure in the Arctic Ocean. *Journal of Geophysical Research*, **96**, 12,725–12,738.

EFRON B. and G. GONG (1983) A leisurely look at the bootstrap, the jackknife, and cross-validation. *American Statistician*, **37**, 36–48.

FOFONOFF N. P. and R. C. MILLARD, JR (1983) *Algorithms for computation of fundamental properties of seawater*. Technical Papers in Marine Science, No. 44, UNESCO Division of Marine Science, Paris, 53 pp.

FOSTER T. D. and E. G. ECKERT (1987) Fine structure, internal waves, and intrusions in the marginal ice zone of the Greenland Sea. *Journal of Geophysical Research*, **92**, 6903–6910.

GARRETT C. J. R. and W. H. MUNK (1975) Space–time scales of internal waves: a progress report. *Journal of Geophysical Research*, **80**, 291–297.

GARRETT C. J. R. and W. H. MUNK (1979) Internal waves in the ocean. *Annual Review of Fluid Mechanics*, **11**, 339–369.

GREGG M. C. (1987) Diapycnal mixing in the thermocline: a review. *Journal of Geophysical Research*, **92**, 5249–5286.

GREGG M. C. (1989) Scaling turbulent dissipation in the thermocline. *Journal of Geophysical Research*, **94**, 9686–9698.

GREGG M. C., E. A. D'ASARO, T. J. SHAY and N. LARSON (1986) Observations of persistent mixing and near-inertial internal waves. *Journal of Physical Oceanography*, **16**, 856–885.

GUEST P. S. and K. L. DAVIDSON (1987) The effect of observed ice conditions on the drag coefficient in the summer East Greenland Sea marginal ice zone. *Journal of Geophysical Research*, **92**, 6943–6954.

HANZLICK D. J. (1983) The West Spitsbergen Current: transport, forcing, and variability. Ph.D. Dissertation, School of Oceanography, University of Washington, Seattle, 127 pp.

HENYEY F. S., J. WRIGHT and S. M. FLATTE (1986) Energy and action flow through the internal wave field: an eikonal approach. *Journal of Geophysical Research*, **91**, 8487–8495.

HUNKINS K. (1986) Anomalous diurnal tidal currents on the Yermak Plateau. *Journal of Marine Research*, **44**, 51–69.

JOHANNESSEN O. M. and B. A. FARRELLY (1984) *MIZEX* 83: *TIROS IR/visual image July* 21, *AXBT from Norwegian* p3, *towed surface temperature, and meteorological data from R.V.* Polarbjorn *and two met./ ocean. buoys* 8 km *apart*. Geophysical Institute, University of Bergen, Bergen, Norway.

JOHANNESSEN O. M., S. SANDVEN, J. A. JOHANNESSEN and S. MYKING (1984) *MIZEX* 83: *Current, temperature, and salinity measurements from drifting ice floes*. Geophysical Institute, University of Bergen, Bergen, Norway.

JOHANNESSEN J. A. *et al.* (1987) Mesoscale eddies in the Fram Strait marginal ice zone during the 1983 and 1984 Marginal Ice Zone Experiments. *Journal of Geophysical Research*, **92**, 6754–6772.

KILLWORTH P. D. and J. M. SMITH (1984) A one-and-a-half dimensional model for the Arctic halocline. *Deep-Sea Research*, **31**, 271–293.

KOWALIK Z. and N. UNTERSTEINER (1978) A study of the M_2 tide in the Arctic Ocean. *Deutsche Hydrographische Zeitschrift*, **31**, 216–229.

KUNZE E. (1985) Near-inertial wave propagation in geostrophic shear. *Journal of Physical Oceanography*, **15**, 544–565.

LEAMAN K. D. and T. B. SANFORD (1975) Vertical energy propagation of inertial waves: a vector spectral analysis of velocity profiles. *Journal of Geophysical Research*, **80**, 1975–1978.

LEVINE M. D. (1983) Internal waves in the ocean: a review. *Reviews of Geophysics and Space Physics*, **21**, 1206–1216.

LEVINE M. D., C. A. PAULSON, M. C. BRISCOE, R. A. WELLER and H. PETERS (1983) Internal waves in JASIN. *Philosophical Transactions of the Royal Society of London*, **A308**, 389–405.

LEVINE M. D., C. A. PAULSON and J. H. MORISON (1985) Internal waves in the Arctic Ocean: comparison with lower-latitude observations. *Journal of Physical Oceanography*, **15**, 800–809.

LEVINE M. D., C. A. PAULSON and J. H. MORISON (1987) Observations of internal gravity waves under the arctic pack ice. *Journal of Geophysical Research*, **92**, 779–782.

MANLEY T. O. (1987) Effects of sub-ice mesoscale features within the marginal ice zone of Fram Strait. *Journal of Geophysical Research*, **92**, 3944–3960.

MARTIN S. and D. J. CAVALIERI (1989) Contributions of the Siberian Shelf polynyas to the Arctic Ocean Intermediate and Deep Water. *Journal of Geophysical Research*, **94**, 12,725–12,738.

MCPHEE M. G. (1984) *Drift velocity during the drift-station phase of MIZEX* 83, MIZEX Bulletin, September 1984, pp. 1–11.

MORISON J. H. (1978) The arctic profiling system. In: *Proceedings of a conference on current measurement*, Technical Report DEL-SG-3-78, College of Marine Studies, University of Delaware, Newark, pp. 311–318.

MORISON J. H. (1980) Forced internal waves in the Arctic Ocean. Ph.D. Dissertation, University of Washington, Seattle, 289 pp.

MORISON J. H., C. E. LONG and M. D. LEVINE (1985) Internal wave dissipation under sea ice. *Journal of Geophysical Research*, **90**, 11,959–11,966.

NESHYBA S., V. T. NEAL and W. W. DENNER (1972) Spectra of internal waves: *in situ* measurements in a multiple-layered structure. *Journal of Physical Oceanography*, **2**, 91–95.

OAKEY N. S. (1982) Determination of the rate of dissipation of turbulent energy from simultaneous temperature and velocity shear microstructure measurements. *Journal of Physical Oceanography*, **12**, 256–271.

OSBORN T. R. (1980) Estimates of the local rate of vertical diffusion from dissipation measurements. *Journal of Physical Oceanography*, **10**, 83–89.

PADMAN L. and T. M. DILLON (1991) Turbulent mixing near the Yermak Plateau during the Coordinated Eastern Arctic Experiment. *Journal of Geophysical Research*, **96**, 4769–4782.

PERRY R. K. and H. S. FLEMING (1986) *Bathymetry of the Arctic Ocean*. Map available from Geological Society of America, Boulder, Colorado.

PINGREE R. D. and A. L. NEW (1989) Downward propagation of internal tidal energy into the Bay of Biscay. *Deep-Sea Research*, **36**, 735–758.

RUDELS B. (1987) *On the mass balance of the Polar Ocean, with special emphasis on the Fram Strait*. Skrifter Nr. 188, Norsk Polarinstitutt, Oslo.

SANDVEN S. and O. M. JOHANNESSEN (1987) High-frequency internal wave observations in the marginal ice zone. *Journal of Geophysical Research*, **92**, 6911–6920.

SANFORD T. B., R. G. DREVER, J. H. DUNLAP and E. A. D'ASARO (1982) *Design, operation and performance of an expendable temperature and velocity profiler (XTVP)*. APL-UW 8110, Applied Physics Laboratory, Seattle, 164 pp.

SMITH W. O. JR, M. E. M. BAUMANN, D. L. WILSON and L. ALETSEE (1987) Phytoplankton biomass and productivity in the marginal ice zone of the Fram Strait during summer 1984. *Journal of Geophysical Research*, **92**, 6777–6786.

TRESHNIKOV A. F. and G. I. BARANOV (1972) *Water circulation in the Arctic Basin*. Monograph, Gidrometeoizdat, Leningrad [(1973) Israel Program for Scientific Translation, Jerusalem, Israel, 145 pp.].

UNTERSTEINER N. (1988) On the ice and heat balance in Fram Strait. *Journal of Geophysical Research*, **93**, 527–531.

WADHAMS P. and V. A. SQUIRE (1983) An ice-water vortex at the edge of the East Greenland Current. *Journal of Geophysical Research*, **88**, 2770–2780.

WADHAMS P., A. E. GILL and P. F. LINDEN (1979) Transects by submarine of the East Greenland Polar Front. *Deep-Sea Research*, **26**, 1311–1328.

WALLACE D. W. R., R. M. MOORE and E. P. JONES (1987) Ventilation of the Arctic Ocean cold halocline: rates of diapycnal and isopycnal transport, oxygen utilization and primary production inferred using chlorofluoromethane distributions. *Deep-Sea Research*, **34**, 1957–1979.

WUNSCH C. (1975) Internal tides in the ocean. *Reviews of Geophysics and Space Physics*, **13**, 167–182.

WUNSCH C. and R. HENDRY (1972) Array measurements of the bottom boundary layer and the internal wave field on the continental slope. *Geophysical Fluid Dynamics*, **4**, 101–145.

YEARSLEY J. R. (1966) Internal waves in the Arctic Ocean. Master's Thesis, Mechanical Engineering Department, University of Washington, Seattle, 62 pp.